Naval Research Laboratory

Washington, DC 20375-5000

NRL Memorandum Report 6630

Experiments with Unsteady, Free Surface, Three-Dimensional Vortices in a Thermally Stable, Stratified Fluid

M. B. STEWART

Center of Fluid Dynamics Development Branch
Laboratory for Computational Physics and Fluid Dynamics Division

S. B. COHEN AND A. W. TROESCH

Department of Naval Architecture and Marine Engineering
The University of Michigan
Ann Arbor, Michigan

May 14, 1990

REPORT DOCUMENTATION PAGE

Form Approved
OMB No. 0704-0188

1. AGENCY USE ONLY (Leave blank)	2. REPORT DATE	3. REPORT TYPE AND DATES COVERED
	1990 May 14	Interim

4. TITLE AND SUBTITLE
Experiments With Unsteady, Free Surface, Three-Dimensional Vortices in a Thermally Stable, Stratified Fluid.

5. FUNDING NUMBERS
PE - 61153N
TA - RR023-01-41
WU - D158-016

6. AUTHOR(S)
Stewart, M. B., Cohen, S. B., and Troesch, A. W.

7. PERFORMING ORGANIZATION NAME(S) AND ADDRESS(ES)
Naval Research Laboratory
Washington, DC 20375-5000

8. PERFORMING ORGANIZATION REPORT NUMBER
NRL Memorandum Report 6630

9. SPONSORING/MONITORING AGENCY NAME(S) AND ADDRESS(ES)
Office of Naval Research
Arlington, VA 22217

10. SPONSORING/MONITORING AGENCY REPORT NUMBER

11. SUPPLEMENTARY NOTES

12a. DISTRIBUTION/AVAILABILITY STATEMENT
Approved for public release; distribution unlimited.

12b. DISTRIBUTION CODE

13. ABSTRACT (Maximum 200 words)

The unsteady characteristics of a vortex pair formed behind a delta wing airfoil at a negative angle of attack have been studied experimentally in a large towing tank with a stable density stratification. Measurements of the vortex pair's upward migration and visualizations of the vortex circulation were made using the hydrogen bubble technique with a laser sheet illumination in the transverse plane. Axial visualizations of the vortex migration and axial velocities at the vortex core were made using the hydrogen bubble technique with a diffuse light source. The effects of the rising vortices and their circulation on the free surface temperature field was recorded using an imaging infrared radiometer mounted over the free surface.

Keywords:

14. SUBJECT TERMS
Free surface flow visualyation hydrogen bubble, Thermal Vortex, Wake detection

15. NUMBER OF PAGES
32

16. PRICE CODE

17. SECURITY CLASSIFICATION OF REPORT	18. SECURITY CLASSIFICATION OF THIS PAGE	19. SECURITY CLASSIFICATION OF ABSTRACT	20. LIMITATION OF ABSTRACT
UNCLASSIFIED	UNCLASSIFIED	UNCLASSIFIED	SR

CONTENTS

EXPERIMENTS WITH UNSTEADY, FREE SURFACE, THREE-DIMENSIONAL VORTICES IN A THERMALLY STABLE, STRATIFIED FLUID

INTRODUCTION

The formation of trailing vortices in the wake of a moving body has long been a subject of considerable interest in aerodynamics, hydrodynamics, and geophysics. The persistent vortices generated by one aircraft at airports is known to pose a hazard to other aircraft using the same runways (Rossow and Tinling 1988). Vortices generated by one part of a body can have a large effect on the response of the body to its downstream control surfaces. This occurs in both aircraft and ships. In addition to lifting surfaces, the junction region between two surfaces joined at a right angle is a common source of trailing vortices (Sung 1987). Surface ships have additional effects caused by a free surface and the effects of a stable density stratification due to temperature or salt concentration gradients (Stewart 1988).

For fluids with a free surface, the trailing vortices formed in the wake of a moving body are three dimensional. In the transverse plane, the fluid motion appears as the swirling motion of the vortex circulation. In the axial plane, there is a large component of fluid velocity in the direction of the generating body at the vortex core. These vortices are very mobile and move in response to other vortices and to the influence of a free surface. Depending on the direction of the circulation, the vortices may rise or fall and, in proximity to a free surface, the vortex can travel some distance along the surface (Sarpkaya 1983).

After formation, viscous forces work very slowly to weaken and diffuse the vortex. The destruction of the initial vortex tube structure is usually caused by an instability. One example is an axisymmetric instability which causes a rapid expansion and deceleration of the transverse and axial velocities. Total circulation remains nearly constant however. Other instabilities are of an axial type and cause the vortex tubes to break and form rings or to attach to the free surface (Sarpkaya 1983).

The presence of a density stratification can reduce the stability of these vortices and effect their overall behavior significantly (Sarpkaya 1983). Attempts to numerically model the vortex-like wake behind a ship caused by the propeller have shown the the results are strongly influenced by the ambient temperature and density stratification (Smith et al. 1986 and Stewart 1988). Previous work with vortices in a density stratified fluid (Sarpkaya 1983) had relatively limited free surface effects because of the deep initial depth of the vortices.

Vortex stability can often be influenced by the techniques used to study them. Anemometer probes and bubbles have been reported to cause premature breakdown in some cases (Sarpkaya 1983). Dye visualizations have been found to change the surface tension characteristics of the fluid and erratically change the behavior of vortices especially near a free surface and possibly near any surface (Willmarth 1988, and Peltzer et al. 1987).

This investigation experimentally measured the formation and evolution of trailing vortices near a temperature and density stratification at the free surface. The effect of these vortices on the free surface is examined and the evolution of the temperature

Manuscript approved February 13, 1990.

history at the free surface is related to the vortex migration. These observations are compared to previous investigations.

EXPERIMENTAL PROCEDURE

Experimental Facility

All measurements were made in towing tank in the Ship Hydrodynamics Laboratory, University of Michigan. Details of this facility are shown in Figure 1. Water depth and tank width in the 3.3m x 6.7m (11 ft. x 22 ft.) cross-section were large enough that sidewall and bottom effects could be neglected. Initial temperature stratification in this tank was measured and determined to be negligibly small. Bulk water temperature was approximately 18 degrees C. For the purposes of this study a temperature stratification in the tank was created by reducing the tank level approximately 0.3 meters and refilling it with the warmer city water supply from the top. The ambient air temperature over the tank was also increased to about 21 degrees C. The water was then allowed settle for one day to minimize the velocity fluctuations and let the temperature profile reach a quasi-equilibrium state. The resulting temperature profile is shown in Figure 2. The first 30 cm has an approximately linear temperature profile with a nearly constant fluid temperature below. Qualitatively this mimics the thermal structure of a large body of water with solar heating and little mixing due to wind or wave action.

Model Description

The model used was a delta wing run at a negative angle of attack. The base was $B = 20$ cm, the length was $h_0 = 28$ cm, and the angle of attack was $\alpha = -12$ degrees. These dimensions were chosen to correspond with a previous study of vortex motion (Sarpkaya 1983) so that comparisons can be made between the two studies. The edges of the model were beveled to a sharp edge. Sarpkaya found noticeable differences in the vortex characteristics when using rounded and sharp edges.

The model was mounted on the towing carriage by a vertical strut piercing the free surface. This arrangement was not optimal either in terms of the flow field or the measurement of the surface temperature but no bottom mounted towing system was available. The strut was beveled on both leading and trailing edges to reduce the disturbance. Observations were made of the thermal disturbance caused by the strut alone and that disturbance was found to be much less than the effect of the rising vortices. The model was submerged to a depth of $D = 46$ cm measured at the model center. At this depth, there was adequate time to observe the rise of the vortices and the migration of the vortices along the surface at all towing speeds used in this study. The results of Sarpkaya (1983) are for $D^* \geq 7.73$ where $D^* = D/b_0$, D is the depth, and b_0 is the initial separation of the vortex pair. In the present results, $D^* = 2.9$. Our results are expected to be influenced by the free surface much more than were seen in the experiments of Sarpkaya.

Data Collection

Data was collected on video tape and analysed using a Macintosh II microcomputer with an image processing board. Vortex circulation and movement were made visible using hydrogen bubbles. Previous investigators have reported that the use of hydrogen bubbles can cause early breakdown of the vortices. Here, we are concerned with the behavior of the vortices before breakdown; the location and type of breakdown are not discussed. The primary alternative to hydrogen bubbles is dye visualization which has a more unpredictable effect especially near a free surface. Because the behavior near a free surface is of primary importance, dye visualization was not considered practical.

The bubbles were generated using a DC power supply at 40 volts and 0.76 mm (.030 in.) wires. These wires were stretched along the top and bottom of each leading edge of the delta wing. This arrangement covered the flow field adequately with bubbles from the top wire and highlighted the core region with bubbles from the bottom wire. The bubbles were then illuminated in one of two ways. For upward migration studies, a vertical, transverse sheet of laser light was generated using a 5 watt argon-ion laser with a vibrating mirror. This arrangement is shown in Figure 3. Images were recorded using an underwater camera to eliminate distortion caused by refraction through the free surface. The camera was mounted on the side of the tank and in front of the laser light sheet. Corrections were made for the viewing angle as a post-processing step using the image processor. Figure 4 is a magnified view of a typical digitized raw image before corrections were applied. The free surface is parallel to a line that connects the two vortex cores. This figure illustrates a typical pixel resolution of about 2mm as used in the tests. Changing the field of view of the video camera determines the ultimate resolution.

Axial views of the vortex behavior were made using an underwater diffuse light source. An example is shown in figure 5. A second video camera was located on an overhead catwalk on the side of the tank. Calibrations were made to correct for view angle so these images could be used to visualize the axial characteristics. Not visible in the still image was the large axial velocity of the vortex cores which could be seen in the video tape.

The temperature distribution on the free surface was measured using an Inframetrics model 600 imaging radiometer. Data was recorded on a standard 1/2 inch video tape. The radiometer was mounted on an overhead support and viewed the horizontal plane directly using a 90 degree surface type look-down mirror. Images were taken of the 8-12 micron infrared emissions and an internal calibration used to convert to temperature. Reflected radiation was reduced by using a 90 degree viewing angle and extinguishing the lights in the towing tank area. The emissivity of water is tabulated at over 0.95 which effectively eliminates the problem of reflected radiation. The temperature measured by the radiometer represents the surface conditions only, since no penetration or depth averaging occurs when recording longwave emitted infrared radiation.

RESULTS AND DISCUSSION

Vortex Behavior

A delta wing moving with a negative angle of attack produces two primary counter rotating vortices which will rise due to the direction of rotation and the mutual influence of each vortex on the other. The rate of rise of the inviscid vortex is given by,

$$V_r = \frac{\Gamma}{2\pi b_0}.$$

Here, V_r represents the rise velocity, Γ the vortex strength, and b_0 is the initial separation distance between the centers of the vortex pair. As the vortices approach a free surface, the effect is the same as if another vortex pair were located on the other side of the free surface. The real vortices will separate and move along the free surface. Classical inviscid fluid theory predicts line vortices will follow a path described by a hyperbola (Lamb 1945). If b_0 is the initial separation and D is the initial depth, line vortices are expected to approach no closer to the free surface than

$$D_{min} = \frac{b_0}{2}\left(1 + \frac{b_0^2}{(2D)^2}\right)^{-1/2}.$$

A delta wing at shallow sumergence would be expected to produce vortices which would approach nearer to the free surface than ones produced at a greater depth. As the vortex pair gradually weakens due to viscous forces, countersign vorticity gradually develops next to the primary vortices which causes them to slow down and move away from the free surface (Wilmarth et al. 1989). At this point, instabilities usually become important and the vortices quickly break down.

In this experiment, the delta wing was towed at three speeds, U = 0.6 m/s, 0.9 m/s, and 1.5 m/s. The value of Γ is estimated from the value of the initial vortex spacing and the rise velocity. The value of Γ for each run is shown in Table 1. A measure of the effects of the density stratification is the Brunt-Vaisala frequency for gravity

$$N^2 = \frac{-g}{\rho_0}\frac{\partial \rho}{\partial y}.$$

To include the effect of vortex strength this is nondimensionalized as the stratification factor $N^* = Nb_0/V_0$. These values are also found in Table 1. In this experiment the effect of the initial depth of vortices on the predicted minimum depth is small in all cases (less than 3 %). Nevertheless, in all cases the vortices came closer than predicted, possibly due to the effect of the stratification. Figure 6 shows the path taken by the vortex centers during these runs. Note that the horizontal scale differs from the vertical scale by a factor of slightly more than three. Although there is a significant difference in Γ for each run, the paths are essentially identical. After tracking parallel to the free-surface for a distance of approximately $2b_0$, the vortex cores begin to travel

downward. This is not explained by current two-dimensional inviscid fluid theories. One hypothesis is that this behavior is caused by contersign vorticity generated by viscous forces. Under clean conditions, vortices near a free surface will generated this secondary vorticity only very slowly due to the zero stress condition (Peace et al, 1983). Vortices approaching a solid surface will generate this secondary vorticity much faster due to the no slip condition at the wall (Barker et al, 1977). Vortices approaching a free surface containing a surfactant concentration gradient experiences a stress condition at the surface between that of a clean free surface and a wall depending on the degree of saturation (Wilmarth et al, 1989).

Figure 7 compares the vortex core displacement with the results of Sarpkaya for the same test configurations. The 45 degree line represents the ideal fluid result for ar. infinitely deep vortex in which the non-dimensionalized total distance, $S^* = S/b_0$ should equal the non-dimensional time, $t^* = tV_0/b_0$, where V_0 is the initial vortex velocity. In the present case the initial dimensionless depth $D^* = D/b_0$ was 2.9 compared to 7.73 used by Sarpkaya. Because of the relatively larger depth, Sarpkaya graphed his results based on H^*, the vertical rise only. The present results are shown on a plot of S^* vs. t^*. This allows a comparison over a longer time. The results are reasonably close. All of the current S^* data lie within the envelope of Sarpkaya's H^* data.

One cause of the scatter in the present data for shallow vortices is that vortex velocity is not constant as it approaches the free surface (Wilmarth et al., 1989). The theoretical velocity calculated using ideal fluid theory reaches a minimum value equal to 1/2 the initial velocity at its closest approach to the intersection of the free surface and the symmetry plane. As it travels along the free surface, it again approaches the initial velocity depending on the initial depth. Figure 8 shows this predicted behavior for a line vortex. Even though the data of Sarpkaya includes only the vortex rise, the vortex cores do not approach close enough to the free surface to be influenced by this effect.

Figure 9 shows the non-dimensional horizontal, W^*, and vertical, H^*, components of the total displacement, S^*, for the right hand vortex core of the slowest run, V = 0.6 m/s. For t^* up to 1.5, H^* is close to the 45 degree line while W^* is virtually flat. For t^* between 1.5 and 2.5, there is a temporary decrease in velocity corresponding to a downward shift in the S^* curve. For t^* larger than 2.5, W^* is parallel to the 45 degree line and H^* is nearly flat. This indicates that all of the rise velocity has changed into horizontal velocity which ultimately approaches the total initial velocity. Beyond t^* larger than 5, the vortices begin to turn downward.

Despite the difference in values of Γ for each run, the paths are essentially identical. The initial separation of the vortices is determined by the geometry of the delta wing which was the same in all cases. Lamb's theory for inviscid line vortices predicts no differences either in the path of the vortices rising to the surface or along the surface. Both are determined only by the initial spacing between vortices and the initial depth. The primary difference in behavior for each run is the velocity at which the vortices move. The vortices generated at the greater tow speed have a larger velocity. Figures 10 a-c show nondimensional plots of velocity, V_r/V_0 vs time, t^*. The vortices all slow

initially as expected and then recover most of the lost velocity after they travel along the surface. The current resolution of the data does not allow a definitive estimate of the effect of the stratified layer on the near-surface behavior of the vortices. Much finer resolution has since become available. Only near the end of each run does the velocity decay, due to viscous dissipation and vortex core breakdown.

Figure 11 shows the axial position of the vortex core for several different times from a position above the free surface and to the side. Here we see the three dimensional characteristic of vortex wandering (Baker 1974), which is seen as a twisting of the vortex core. This type of behavior leads anemometry measurements to overestimate vortex size when time-averaging.

Thermal Disturbance

As the vortices rise through a temperature stratified fluid they carry subsurface water to the surface via two processes. The first occurs during the initial roll-up of the vortices, when fluid at the initial depth is captured and carried during the entire history of the vortex. The second occurs outside the vortex, when nearby fluid is pumped upward by each vortex and stays at the temperature corresponding to the original location of the vortex. As the two vortices spread along the surface this cooler water will remain between them.

Figures 12 a-c show three distinct stages in development of the surface temperature disturbance. Figure 12a shows the initial appearance of the disturbance as the vortices first arrive at the surface. Because of the direction of the circulation, the cold water first appears at the centerline. In addition, the shape of the disturbance at this phase is strongly aligned in the horizontal, transverse direction. This three-dimensional behavior has been observed previously in the surface elevations as the vortices rise to the surface (Sarpkaya 1987, and Wilmarth et al. 1989).

Figure 12b shows the characteristic of the surface disturbance as the vortices begin to spread along the surface. Here the disturbance follows the spread of the vortices. The three dimensional transverse structure of the disturbance is mostly seen at the edges. The center of the disturbance continues to cool until either the minimum deep water temperature is reached or the vortices separated sufficiently and the fluid velocities at the center stop. Temperature gradients at the edges of the disturbance are very sharp.

Figure 12c shows the disturbance after the vortex breakdown. Here the time scales are much larger as the cooler water at the surface slowly sinks and the warmer water covers the disturbance. The predominately two dimensional structure of the disturbance degenerates to a very irregular pattern before disappearing. The temperature gradients become less distinct as the larger time scales involved allow diffusion to become important.

As a comparison between these measurements and the behavior seen in the ocean, Figure 13 shows infrared images of a ship's wake made at a time when the thermal structure of the ocean was qualitatively similar to the current laboratory experiments. The temperature disturbance is very similar in both cases. This similarity is even more

striking because of the quantitative differences in the structure of the flow. In each case there is a large component of swirl velocity which is the primary cause of the temperature disturbance. However, in a ship wake, the fluid structure is much more complex with a decaying turbulence field, an axial velocity field which is qualitatively different, and possibly more secondary flow structures. Nevertheless, the beginning, the spread, and the decay, are well represented in the ship wake.

An analysis was carried out to see if the three stages of thermal surface disturbance could be recognized by either a change in the boundary between thermal gradients, or a change of the boundary with time. The boundary was characterized by its fractal number based on the "grid dimension method" (Peitgen et al. 1988) and found to be 1.47 +/- 2%, independent of temperature or time. The grid method was chosen to overcome the inability to determine a connected boundary from a video image. Typically, the infrared image contained 6 to 10 pixels along each scan line that could be interpreted as the edge of the temperature gradient. Trying to chose one and connect it to the next scan line is nearly impossible without some type of smoothing algorithm which may radically change the fractal value. The grid method simply identifies whether or not a boundary point is within the test grid. For moderate size grids, the extra points per scan line have little effect. However, it is expected that the fractal value is somewhat overstated since no filtering or smoothing was done to the video images before analysis.

CONCLUSIONS

The unsteady behavior of trailing vortices from a delta wing air foil at negative angle of attack near a temperature and density stratification has been studied experimentally. The path of the vortices as they approach and spread along the free surface generally follow inviscid line vortex theory. They did approach $10 - 20\%$ closer to the free surface and eventually moved deeper and broke down which is not predicted by inviscid theory. The qualitative trends in the vortex migration velocity are well predicted by inviscid theory. These effects were independent of a three fold change in vortex strength. Final vortex core downward velocity and breakdown appear to be strongly influenced by viscous effects. These viscous effects occur even without surface tension forces but the presence of a surfactant gradient would make viscous effects occur much sooner. For the range of stratification parameters, $N^* = 0.16$ to 0.32 studied here, the effects of the density stratification were small, however disturbances on the surface were seen to have very sharp edges. These edges have a fractal dimension of approximately 1.47 independent of temperature or time Similar fluid structures caused by propellers become hydrodynamically unstable when modeled numerically. This behavior was not seen in these experiments. The effects over time of these shallow vortices on the surface temperature disturbance is seen to have 3 stages: transverse three dimensional behavior; outwards spreading; and two dimensional degeneration. These are qualitatively quite similar to full scale observations behind a ship.

ACKNOWLEDGEMENTS

This work was supported by the Office of Naval Research (Code 12) and the Naval Research Laboratory under the Fluid Dynamics Task Area.

REFERENCES

1. Baker, G. J., Barker, S. J. Bofah, K. K. and Saffman, P. G., (1974), J. Fluid Mech., Vol. 65
2. Barker, S. J., and Crow, S. C., (1977), J. Fluid Mech., Vol. 82
3. Lamb, H., (1945), *Hydrodynamics*, Sixth Ed., Dover
4. Peace, A. J., and Riley, N., (1983), J. Fluid Mech., Vol. 129
5. Peitgen, H. O., et al., Editors, (1988), *The Science of Fractal Images*, Springer-Verlag, New York.
6. Peltzer, R. D., Garrett, W. D., and Smith, P. M., (1987),"A Remote Sensing Study of a Surface Ship Wake", Int. J. Remote Sensing, Vol.8, No.5
7. Rossow, V. J., and Tinling, B. E., (1988), "Research on Aircraft/Vortex-Wake Interactions to Determine Acceptable Level of Wake Intensity", J. Aircraft, Vol.25, No.5
8. Sarpkaya, T., (1983), "Trailing Vortices in Homogeneous and Density-Stratified Media", J. Fluid Mech., Vol.136
9. Sarpkaya, T., and Daly, J. J., (1987), "Effect of Ambient Turbulence on Trailing Vortices", J. Aircraft, Vol.24, No.6
10. Smith, R. W., Hyman, M. C., and Uzes, C. A., (1986), "Bubble Transport in Ship Wakes with Application to Wake Modification", NCSC TM, U4210-86-29-40U17, Naval Coastal Systems Center, Panama City, Fla.
11. Stewart, M. B., (1988), "Numerical Predictions of Thermal Ship Wakes", The Eleventh Annual Energy Sources Technology Conference and Exhibition, New Orleans.
12. Stillinger, D. C., Helland, K. N., and Van Atta, C. W., (1983), "Experiments on the Transition of Homogeneous Turbulence to Internal Waves in a Stratified Fluid", J. Fluid Mech, Vol.131
13. Sung, C. H., (1987), "An Explicit Runge-Kutta Method for 3D Turbulent Incompressible Flows", DTNSRDC/SHD-1244-01, David Taylor Research Center, Bethesda, Maryland.
14. Wilmarth, W., and Hosa, E.,(1989), personal communication.

TABLE OF SYMBOLS

Dimensional	*Non − dimensional*
B = Delta wing chord length at base	
b_0 = Vortex separation distance	
D = Initial depth of vortices	$D^* = D/b_0$, Relative depth
d = depth	
g = Acceleration of gravity	
H = Vertical rise of vortices	$H^* = H/b_0$, Relative rise
h_0 = Length of delta wing	
N = Brunt-Vaisala frequency for gravity	$N^* = Nb_0/V_0$, Stratification factor
S = Total displacement of vortex $= [H^2 + W^2]^{1/2}$	$S^* = S/b_0$, Relative displacement
T = Temperature (Celsius)	$T^* = (T - T_d)/(T_s - T_d)$
T_d = Deep water temperature (Celsius)	
T_s = Surface temperature (Celsius)	
t = Time	$t^* = tV_0/b_0$, Normalized time
U = Model velocity	
V_r = Vortex rise velocity	$V^* = V_r/V_0$, Migration velocity
V_0 = Initial vortex rise velocity	
W = Horizontal spread of vortices	$W^* = W/b_0$, Relative spread
α = Angle of attack	
Γ = Vortex strength	$Re = \Gamma/\nu$, Reynolds number
ρ = Mass density	
ν = Kinematic viscosity	

TABLE 1

Tow Speed $U\,(m/s)$	Reynolds No. Re	Migration Vel. $V_r\,(cm/s)$	Vortex Strength $\Gamma\,(cm^2/s)$	Stratification $N^* = Nb_0/V_0$
0.6	23000	2.5	251	0.32
0.9	33000	3.6	362	0.27
1.5	63000	6.9	694	0.16

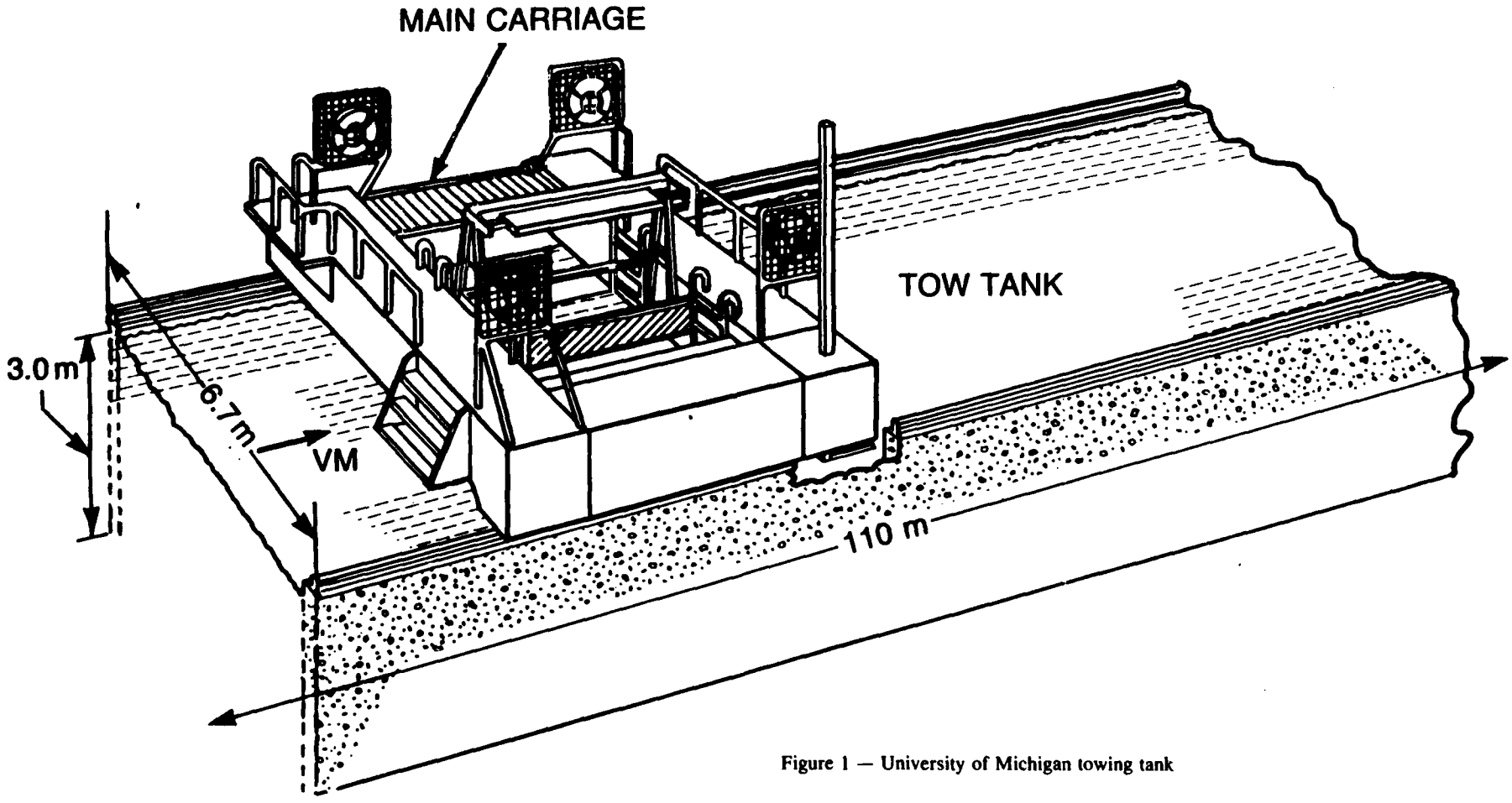

Figure 1 — University of Michigan towing tank

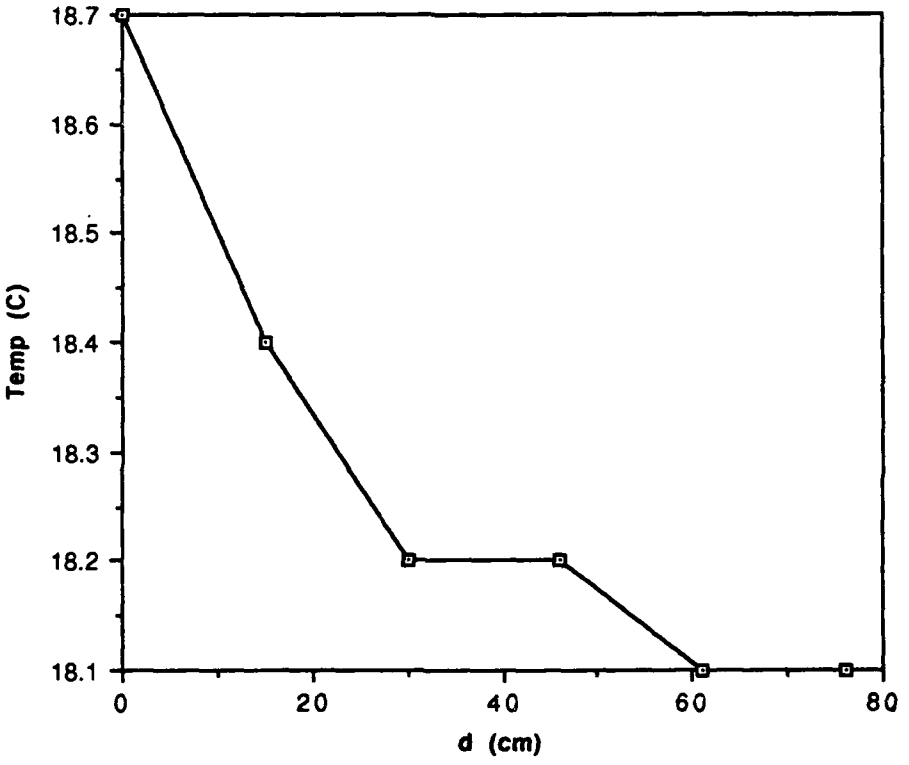

Figure 2 — Temperature stratification

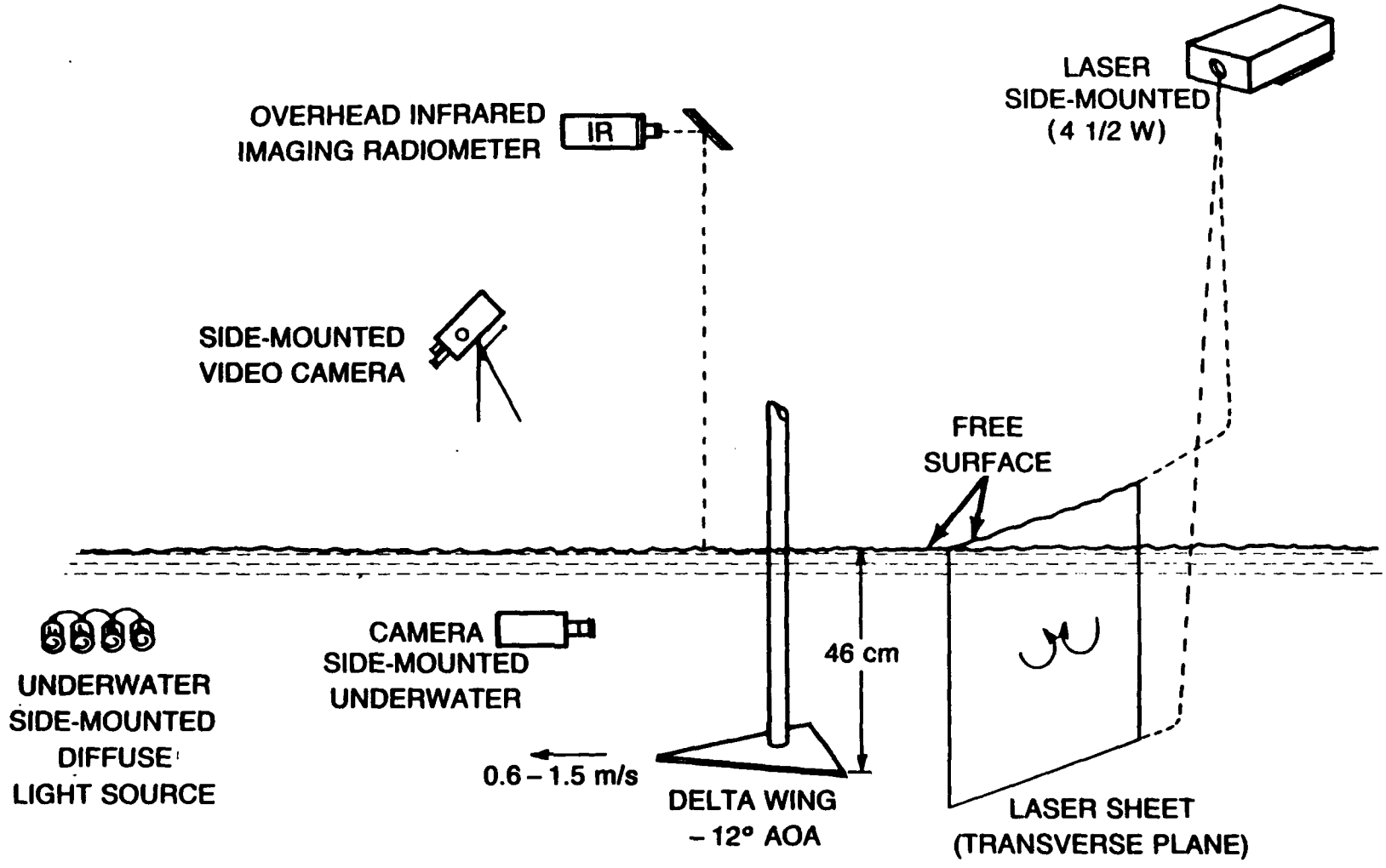

Figure 3 — Exerimental data collection

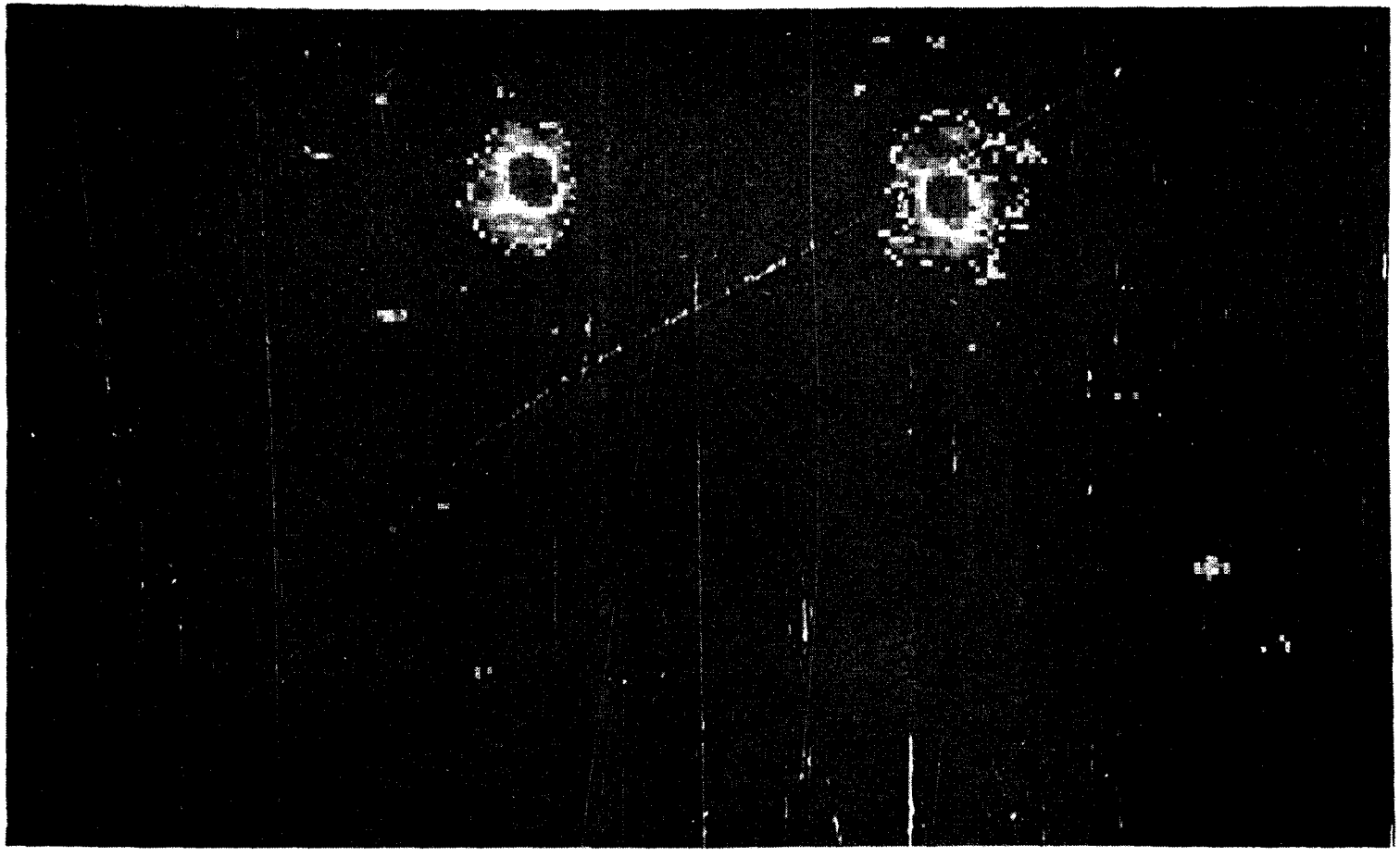

Figure 4 — Digitized video image of laser illuminated vortices

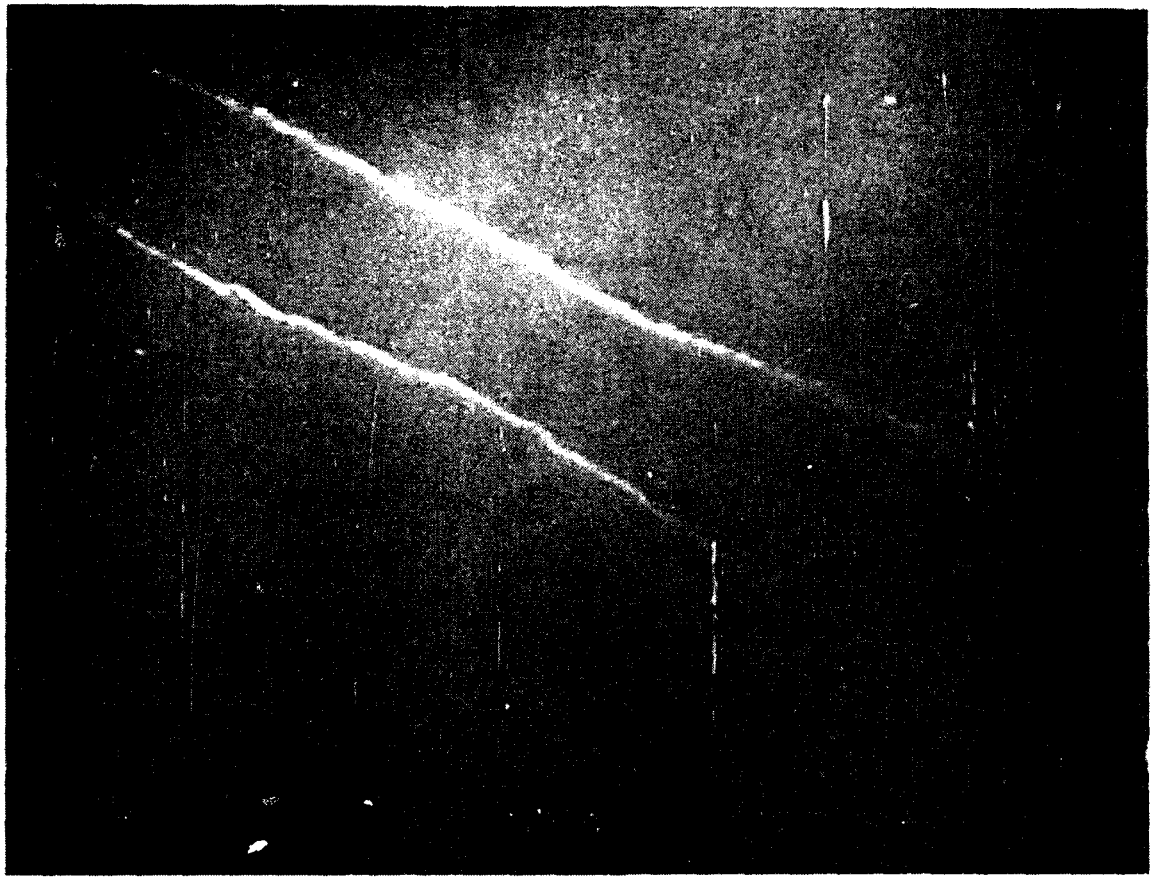

Figure 5 — Axial video image of vortex lines

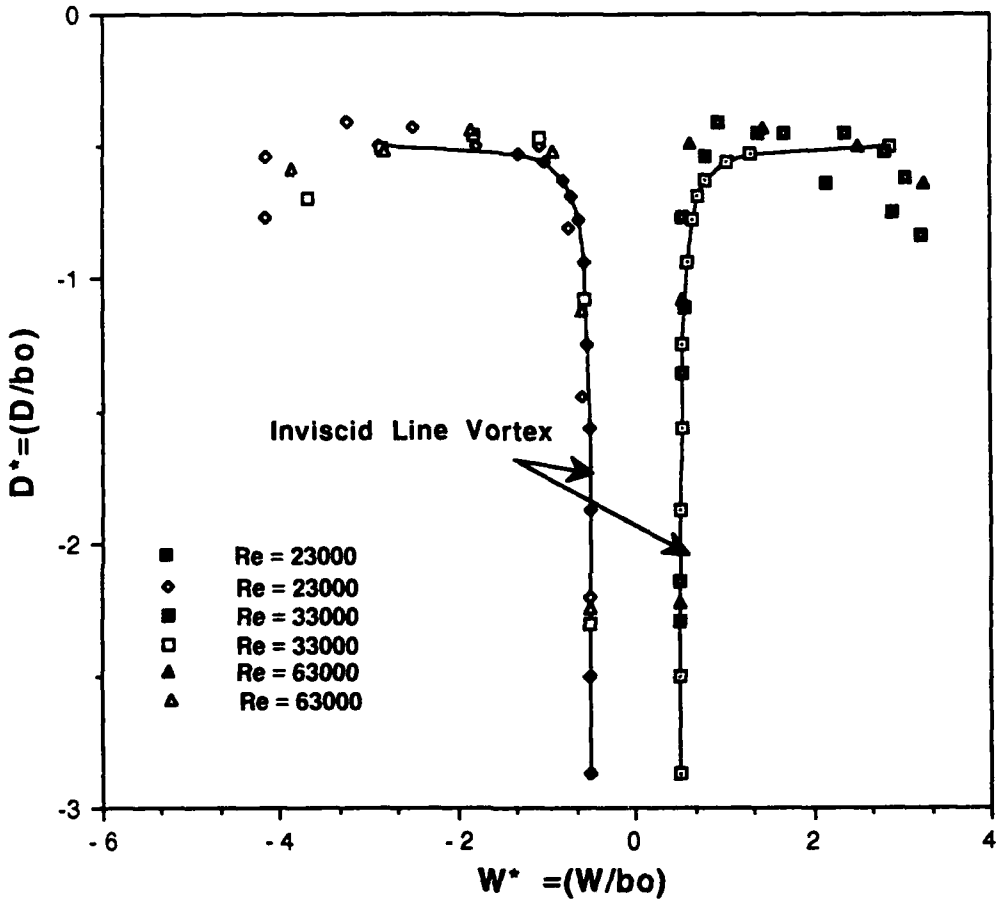

Figure 6 — Vortex core position
Re = 23000-63000

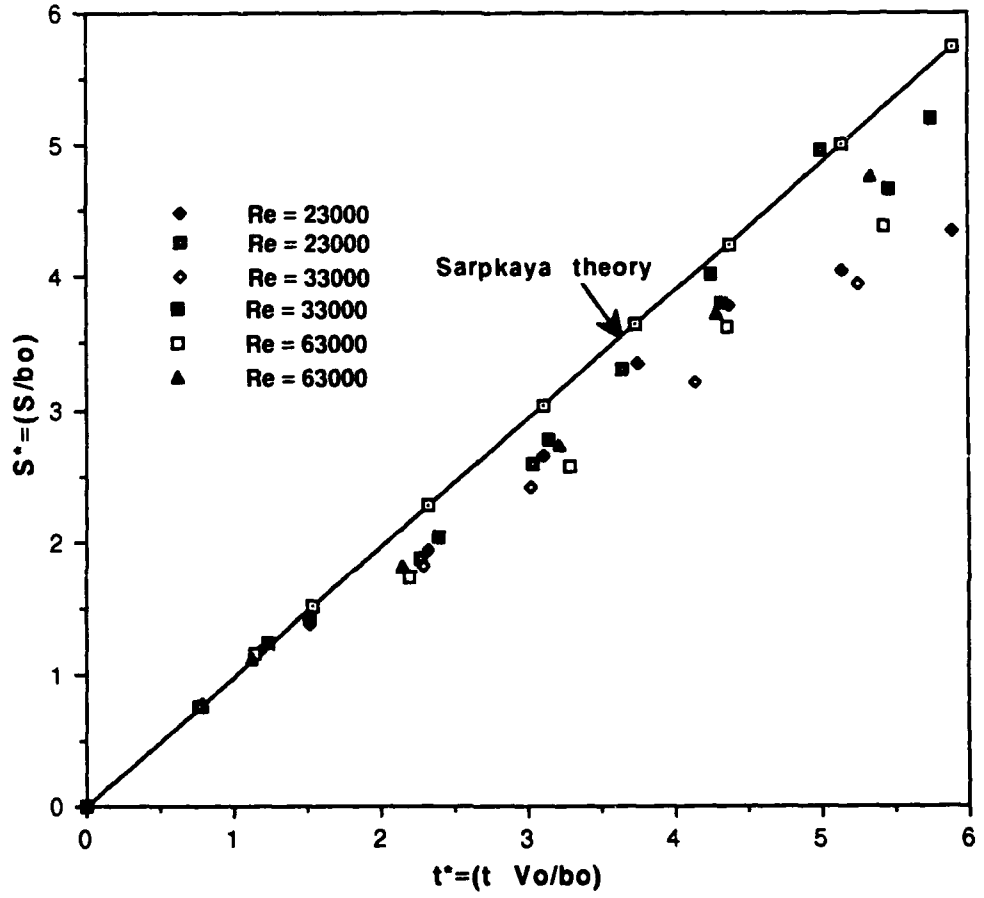

Figure 7 — Vortex core displacement vs time

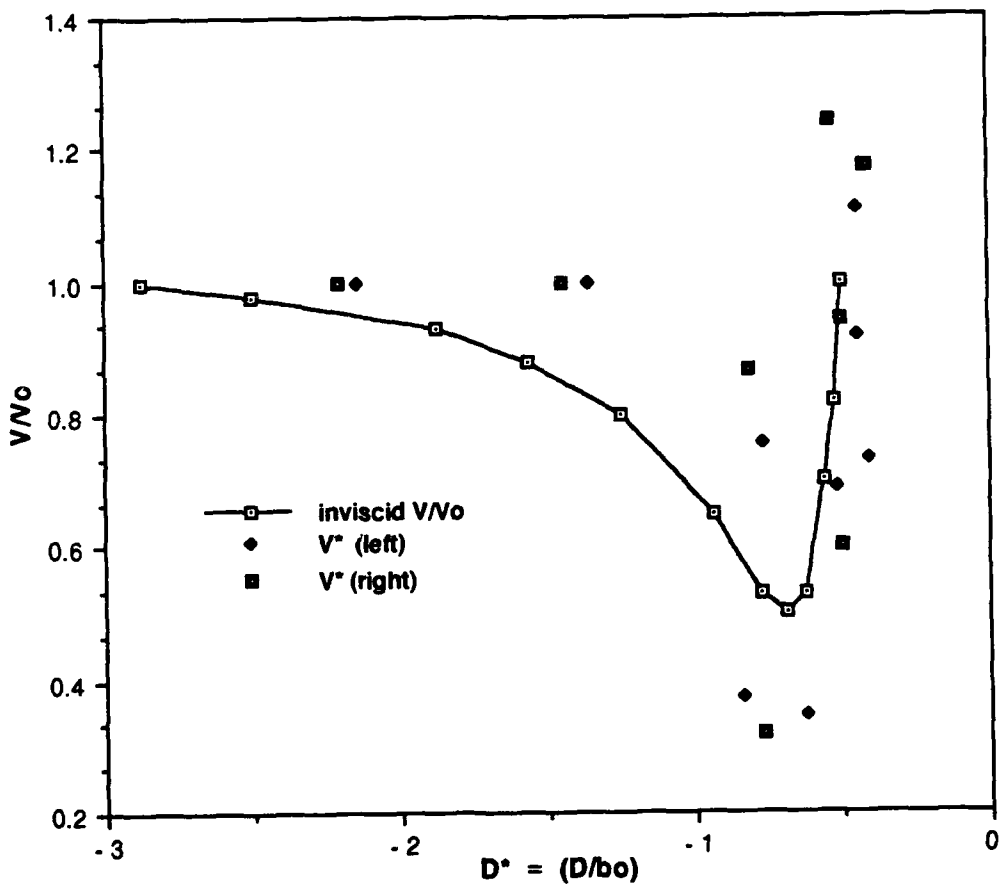

Figure 8 — Vortex core velocity vs depth
$Re = 23000$

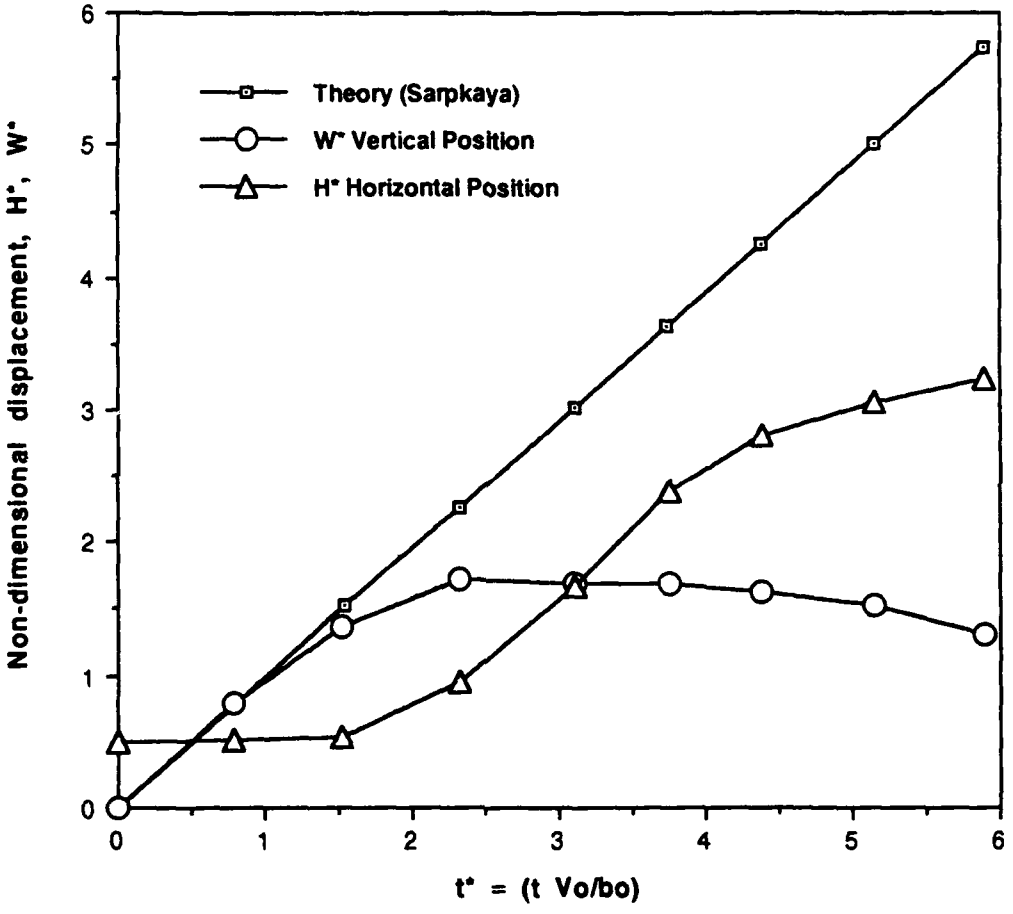

Figure 9 — Vortex core rise and spread
Re = 23000

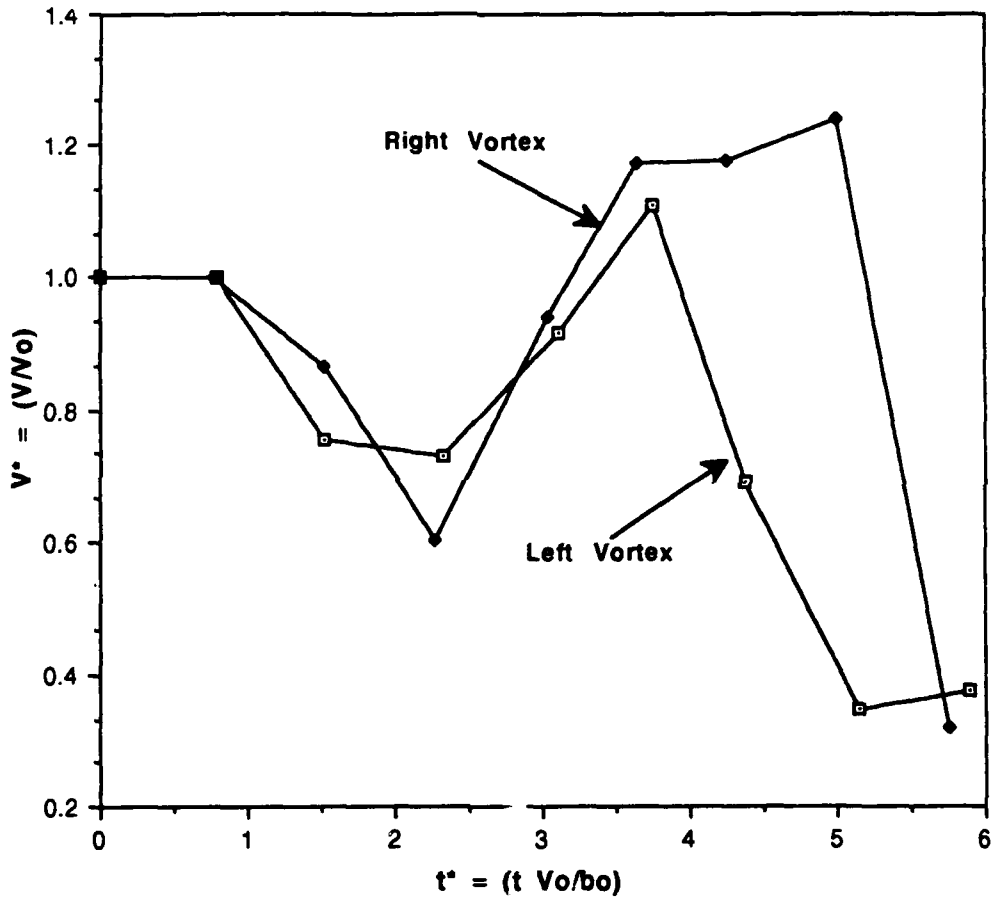

Figure 10a — Vortex velocity vs time
Re ≈ 23000

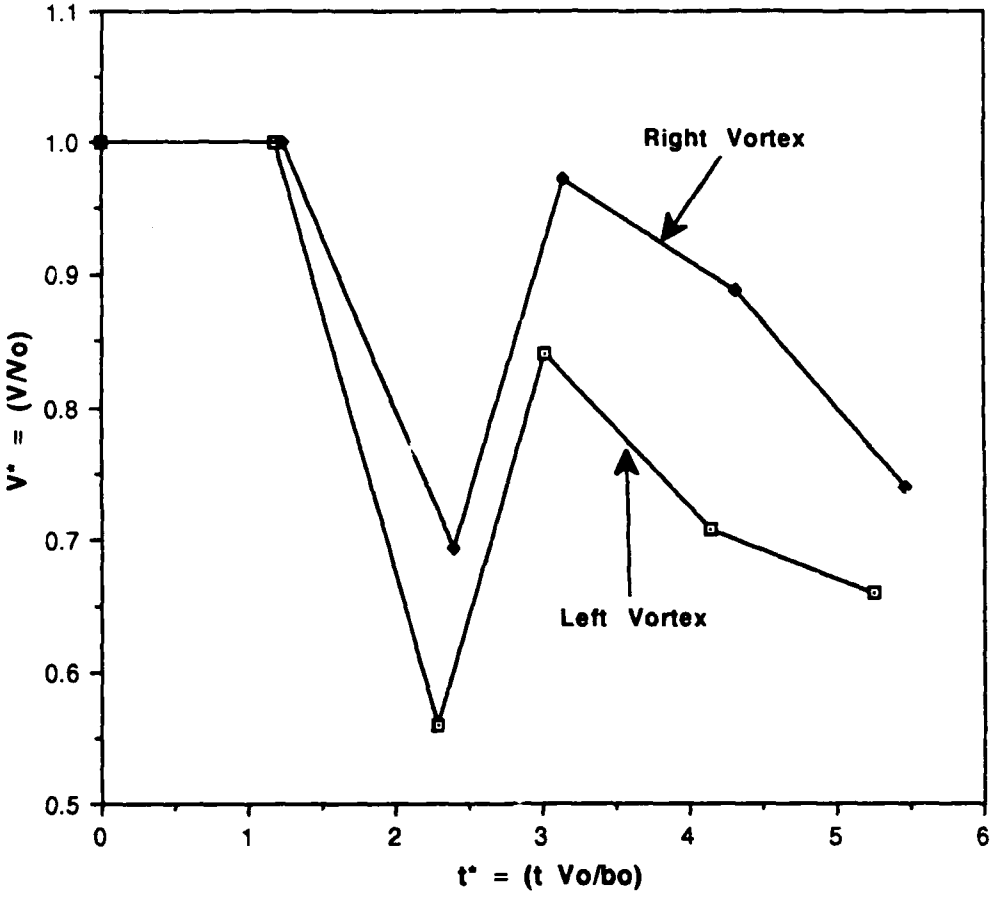

Figure 10b — Vortex velocity vs time
Re = 33000

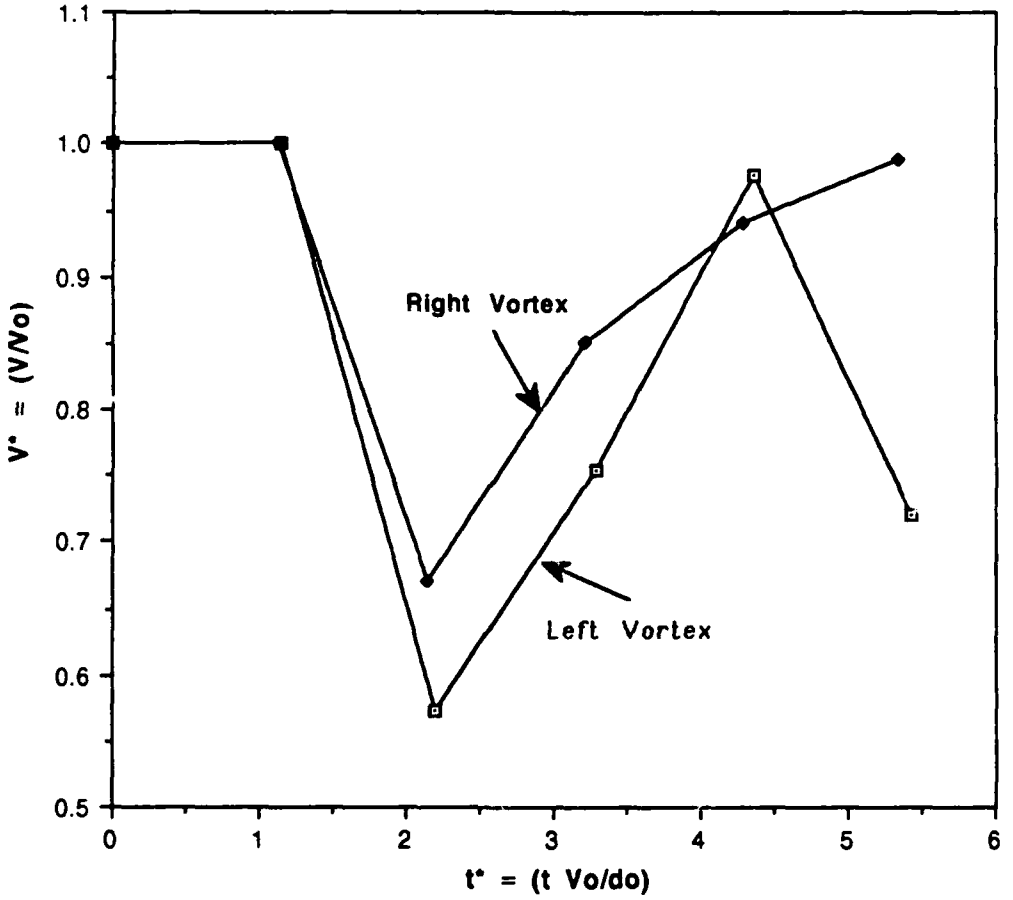

Figure 10c — Vortex position vs time
Re = 63000

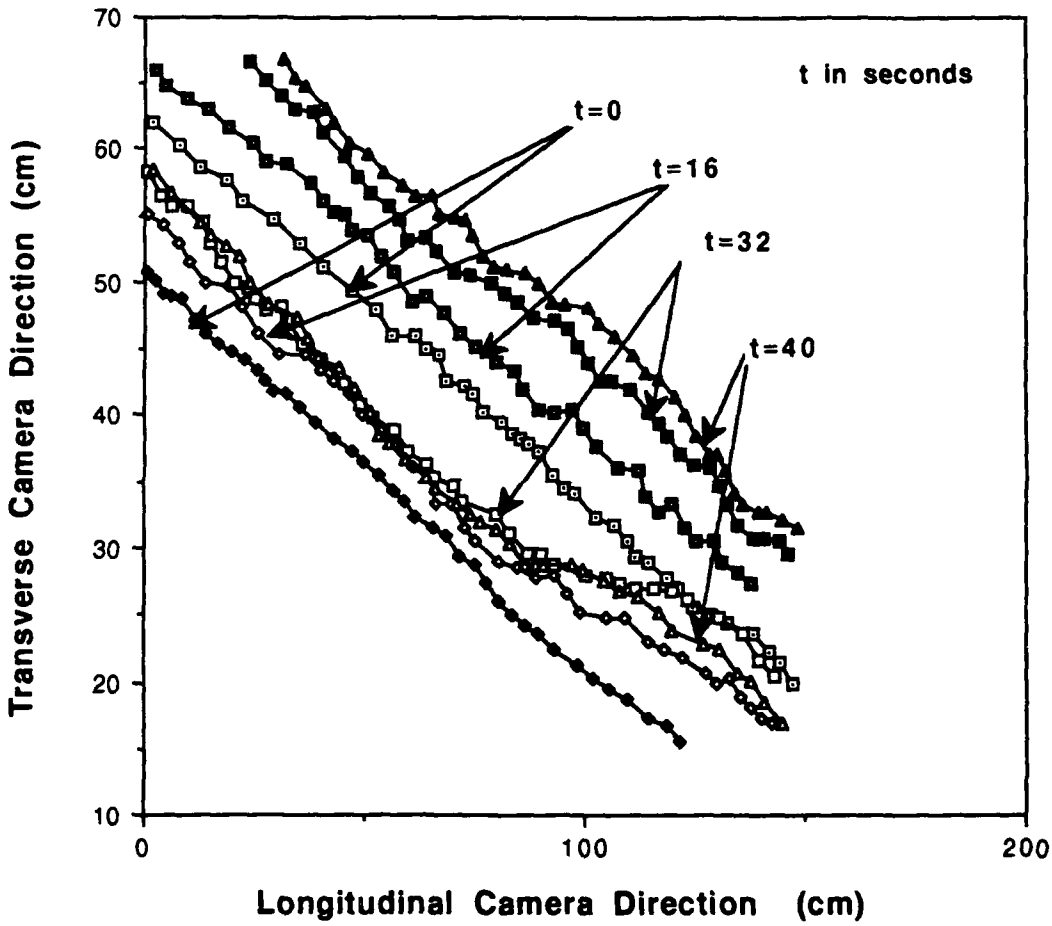

Figure 11 — Vortex lines at 0.6 m/s

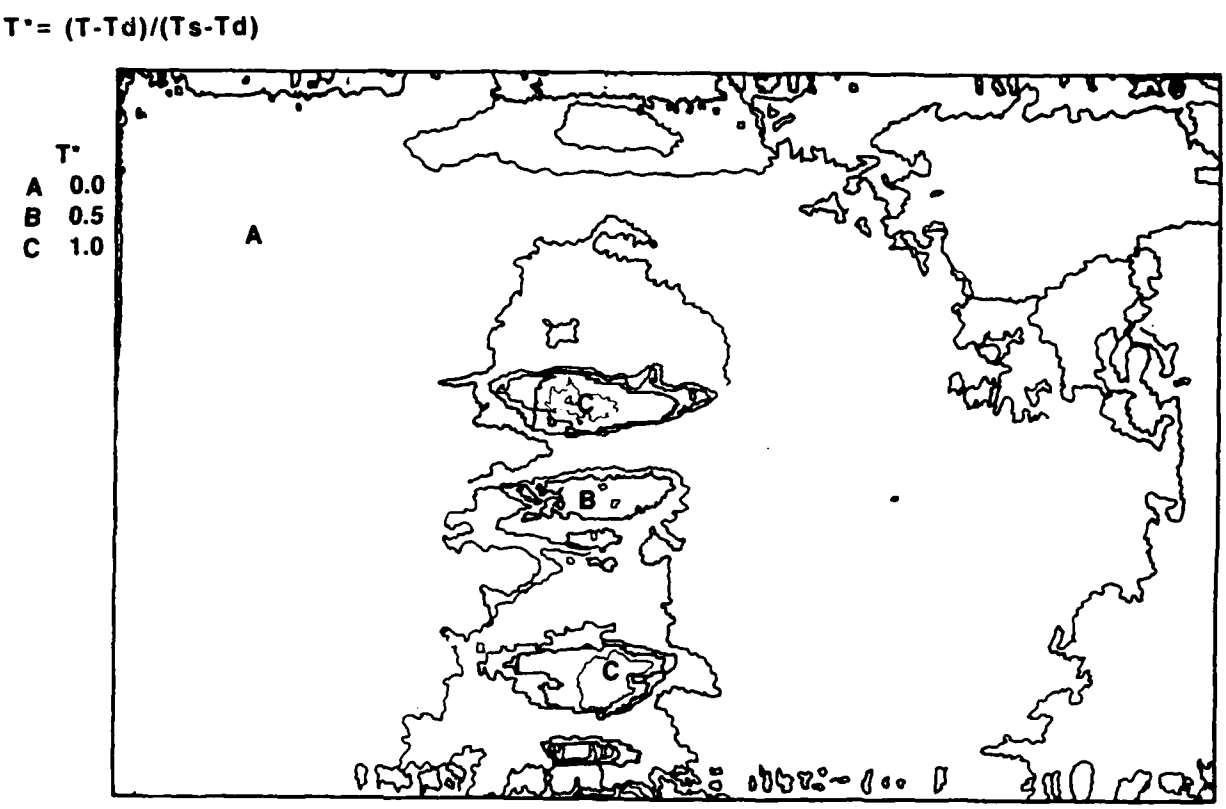

Figure 12a — Surface temperature as the vortex approaches free surface

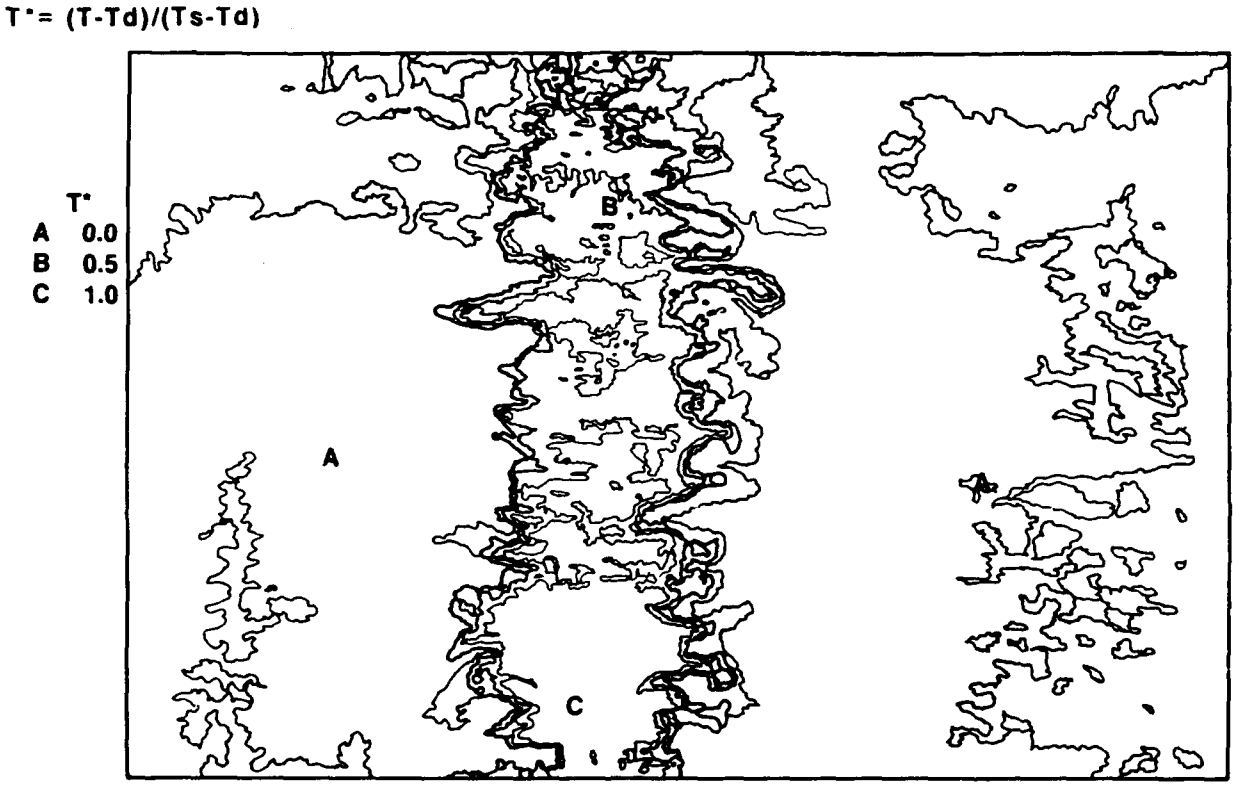

Figure 12b — Surface temperature during vortex spreading

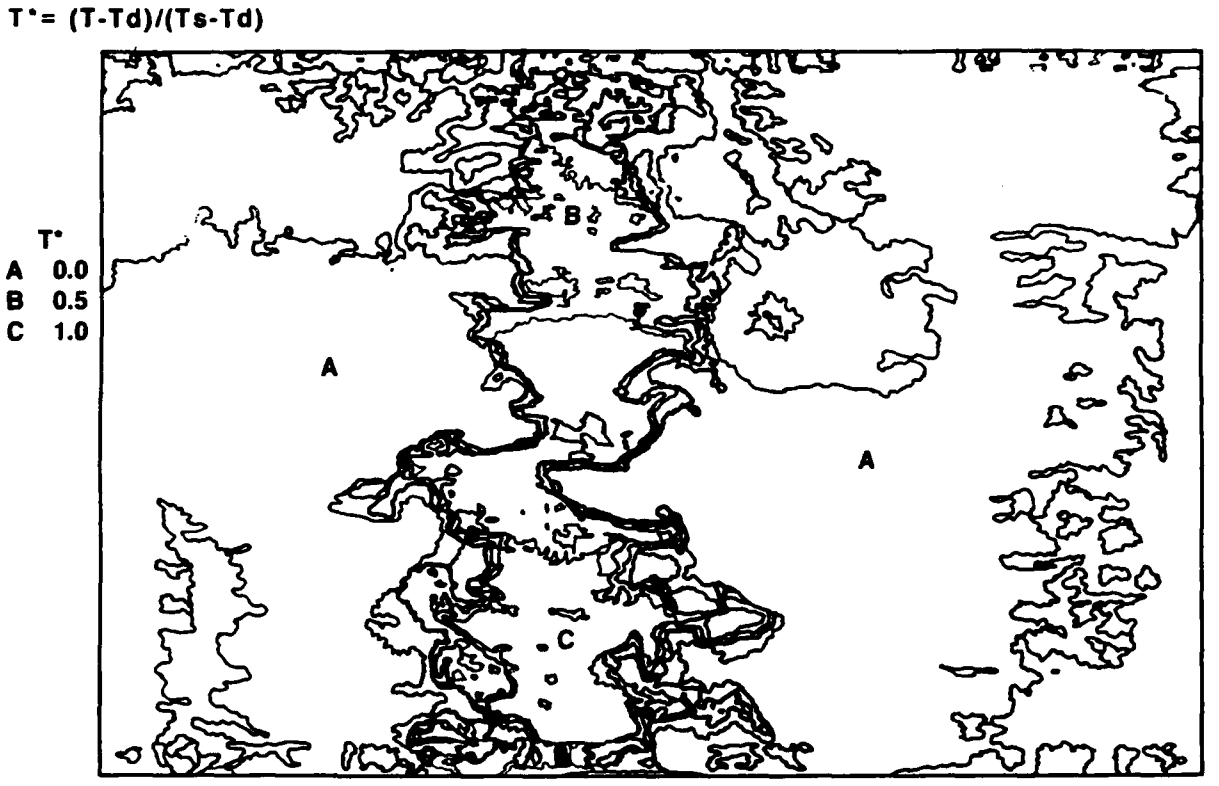

Figure 12c — Late surface temperature wake decay

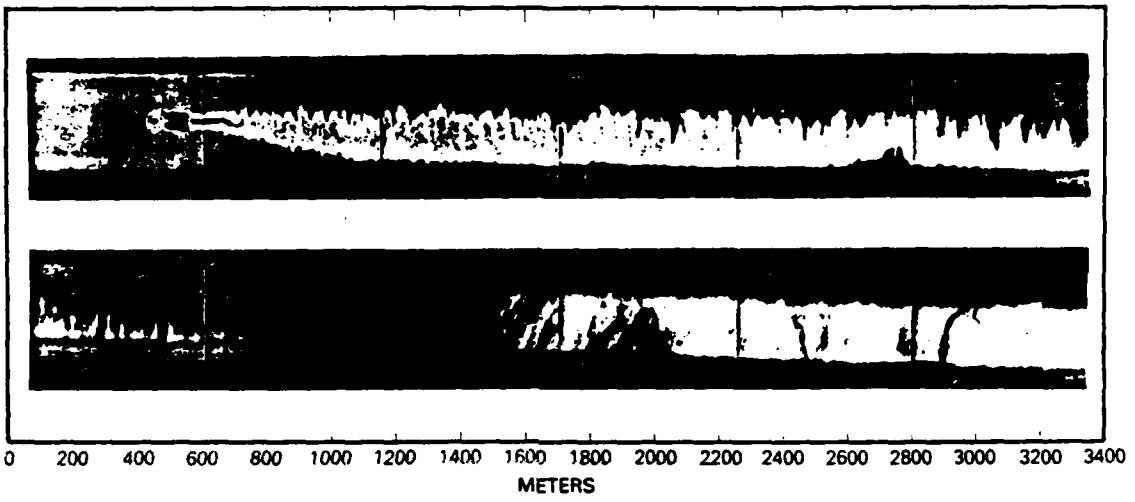

Figure 13 — Thermal image of ships wake